JOURNAL OF CATALYSIS 130, 627–641 (1991)

# Depth Profiling of Catalyst Samples: An XPS-Based Model for the Sputtering Behavior of Powder Materials

AGUSTIN R. GONZÁLEZ-ELIPE, JUAN P. ESPINÓS, ASUNCIÓN FERNÁNDEZ, AND GUILLERMO MUNUERA

*Instituto de Ciencia de Materiales de Sevilla and Departamento de Química Inorgánica, CSIC-Universidad de Sevilla, P.O. Box 1115, 41071 Sevilla, Spain*

Received April 27, 1990; revised March 8, 1991

A model is presented to describe the depth profiles obtained by ion-bombarding polycrystalline multicomponent samples. Different calculations for idealized catalyst structures illustrate the possibilities of using the ion-sputtering technique for the characterization of catalysts. These calculations show that the depth profiles obtained using dispersed phase XPS intensities may provide semiquantitative information on particle size, existence of solid solution, or formation of mono- or bimetallic particles in bimetallic catalysts. Examples with the dispersed phase in metallic or oxide forms that illustrate these applications are presented. © 1991 Academic Press, Inc.

## INTRODUCTION

The use of ion sputtering is a common tool in surface analysis which, in combination with surface-sensitive techniques such as AES, XPS, ISS, or SIMS, provides information on the in-depth distribution of elements in solid samples (*1*). This technique has found many applications in materials where some inhomogeneity in composition occurs in the topmost layers, being extensively used to study phenomena such as surface segregation, corrosion, and surface passivation.

For compact materials a first simulation of the surface etching rate and of the measured composition profile was developed by Benninghoven (*2*), who proposed the so-called sequential layer sputtering model (SLS). This model assumes that the analyzed material is formed by layers of different composition and size and that the coverage degree of any layer by those on top of it increases from the surface to the bulk.

However, ion sputtering is a destructive technique which induces considerable modifications in the surface composition and morphology, so that the measured in-depth composition is a convolution of the true composition and the results of phenomena like cratering (*3*), preferential sputtering (*4*), and atom implantation (*5*). To take into account these and other factors several improvements of Benninghoven's model have been proposed, which consider additional parameters like the mean free path of electrons in the case of using XPS or AES as analytical techniques (*6*), preferential sputtering yields (*7*), and the dependence of the etching rate on the coordination state of the atoms at the surface (*8*).

However, the use of the sputtering techniques to study powder specimen or materials with a globular structure (cermet or composite materials) has been more limited. Thus, although some studies have been carried out on catalysts (*9–11*), minerals (*12*), or Brown coals (*13*) the derived conclusions have been partially intuitive and of qualitative character.

Similarly, only very few models have been developed to interpret the sputtering behavior of these kinds of materials. Among them we can mention the model of Henrich and Fan (*14*) for MgO/Au cermets based on the different sputtering yields of the two



0021-9517/91 $3.00

components, that of Cross and Dewing (*15*) to determine the thickness of $SiO_2$ layers covering spherical particles of $TiO_2$, or that of Nyborg *et al.* (*16*) to estimate the oxidized thickness of spherically shaped metal powders.

In the present work, a semiquantitative model is worked out trying to explain the sputtering profiles obtained by XPS with specimens in powder form. In principle, the model has been conceived in relation to problems of catalyst characterization and, consequently, the selected examples come from this field. However, its area of application can be extended to investigate other composite or powder materials, where one of the phases is highly dispersed in the matrix or on the surface of a carrier support.

Some not necessarily true restrictions have also been assumed in the model in order to simplify its mathematical formulation. Thus, no preferential sputtering, ion implantation, or phase diffusion phenomena have been taken into account. However, we think that in a first approximation such factors can be neglected because other phenomena of similar importance, such as sample inhomogeneity and surface roughness, cannot be estimated for these materials.

To validate the model a series of examples are presented that illustrate the possible applications of this technique for the characterization of catalysts. When possible, the results are contrasted with data obtained by other characterization methods, thus showing the range of validity of the sputtering technique.

## MODEL DESCRIPTION

Figure 1 shows a schematic representation of a catalyst sample consisting of big particles of a support and small particles of a dispersed phase deposited on them. In principle, the dispersed phase could be a metal, an oxide, or a sulfide, although the forthcoming formulation is given for supported metal catalysts. For the electron energy analyzer (EEA) placed perpendicular to the sample, the particle structure of this

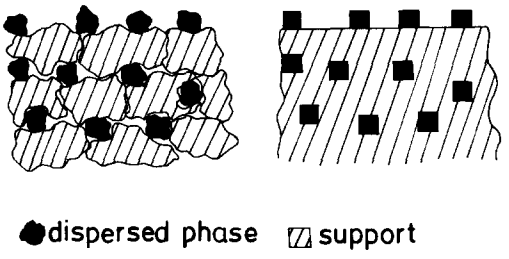


FIG. 1. Left: Representation of a catalyst sample formed by big particles of a carrier and small particles of a dispersed phase. Right: Idealization of this structure as seen by the electron energy analyzer.

catalyst is equivalent to the globular structure also presented in the same figure where, for simplicity, a cubic shape and the same size is assumed for all the particles of the active phase. Implicit in all the formulations is that the particle size of the dispersed phase is much smaller than that of the support (see Apendix). Basic parameters of the catalyst sample used in the model are:

$S_{bet}$: Specific surface of the support ($m^2$ $kg^{-1}$)

$\rho$: specific weight of the support (kg $m^{-3}$)

$d$: size of the particle of the dispersed phase taken as cubic (m)

$D_m$: atomic bulk density of the dispersed phase (atoms $m^{-3}$)

$\rho_2$: surface concentration of atoms of the dispersed phase referred to the surface of the support (atoms $m^{-2}$).

### *Photoelectron Peak Intensities before Sputtering*

In the globular representation in Fig. 1 it can be considered that there are two different contributions to the XPS intensity of any photoelectron peak produced by the dispersed phase: First, that of the particles exposed at the surface and, second, that corresponding to those particles embedded in the matrix formed by the support. For convenience, in the following, these two parts are referred to as "surface" and "bulk" of the specimen. The contribution of the surface can be estimated as

$$I_s \alpha\, Ad^2(1 - \exp(-d/\lambda_m)), \qquad (1)$$

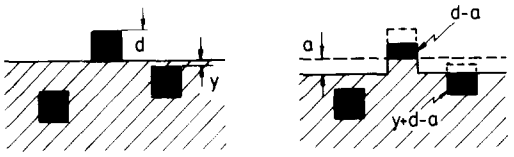


FIG. 2. Effect of $Ar^+$ sputtering on the idealized catalyst structure. Left: Before sputtering. Right: after removal of a thickness "a" from the sample.

where $\lambda_m$ is the mean scape depth of the photoelectron through the dispersed phase, $d^2$ is the area of a face of the cubic particles of the dispersed phase, and $A$ is the number of particles per unit area of sample (i.e., referred to the macroscopic surface of sample seen by the EEA). An approximate value for $A$ is derived in the Appendix by assuming a spherical shape for the particles of the support. However, in general, $A$ can be taken as an adjustable parameter.

To estimate the contribution of the bulk to the peak intensity, the attenuation of the photoelectrons before escaping the surface must be taken into account. For the sake of simplicity we assume that this attenuation is produced entirely by the support, i.e., that the probability that two particles at different depths are at the same lateral position is practically zero. Under this assumption, the contribution to the photoelectron intensity of the buried particles in Fig. 1 is

$$I_b(y) \alpha D d^2(1 - \exp(-d/\lambda_m)) \exp(-y/\lambda_s), \quad (2)$$

where $\lambda_s$ is the attenuation length of the photoelectrons of the dispersed phase through the support and $D$ the number of particles at a depth "$y$" in a layer of area unity and thickness $dy$ (Fig. 2). The value of $D$ has been calculated in the Appendix for the case of the closed-packed structure of spheres in Fig. A1. However, as for the parameter $A$ in expression (1), $D$ can be taken as an adjustable parameter. Changes in the relative values of $A$ and $D$ in respect to those calculated according to (A3) and (A9) would indicate either a surface segregation of the active phase or its preferential distribution in the pores of the support (see Appendix).

Integration of expression (2) throughout the total sample depth gives

$$I_b \alpha D d^2 \lambda_s (1 - \exp(-d/\lambda_m)). \quad (3)$$

So, the total intensity of the photoelectron peak for our metallic catalyst before sputtering would be

$$I = I_b + I_s \alpha (d^2(1 - \exp(-d/\lambda_m))(A + D\lambda_s). \quad (4)$$

In principle, this simple expression should give an account of the relative intensity of peaks of the dispersed phase in function of parameters like $d$ and $\rho$ (the first one related to the degree of dispersion). In this sense we have checked this expression (4) to estimate the Ni(2$p$) relative intensity for a series of $Ni/SiO_2$ catalysts with different metal loading and dispersions, showing that the calculated values were in acceptable agreement with the experimental ones (*17*). However, it is important to stress here that, in the present work, expression (4) is used as a starting point to describe the effect of the ion sputtering on a catalyst sample, and that much more elaborate models exist in the literature aiming an accurate prediction of the experimental peak intensities (*18–20*).

*Effect of the $Ar^+$ Sputtering*

Assuming a layer by layer sputtering of the idealized globular structure in Fig. 1 the situation in Fig. 2 would occur after sputtering for a time $t$ corresponding to the removal of a thickness $a$ of sample. If $a < d$ the intensity of the photoelectron signal corresponding to the particles at the surface, now of thickness $d - a$, should be

$$I'_s \alpha A d^2 (1 - \exp(a - d)/\lambda_m). \quad (5)$$

Meanwhile, at the bulk, some particles which were covered by the support before sputtering are now exposed and partially etched, their height being $y + d - a$ as seen in Fig. 2. The contribution of these particles to the intensity of the XPS signal can be

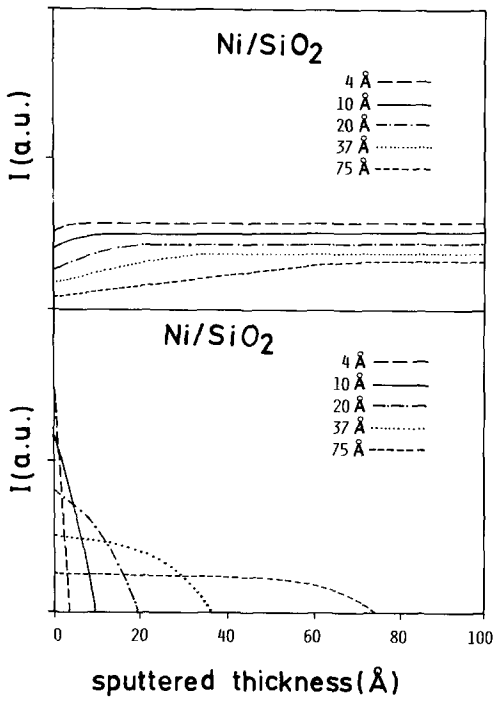


FIG. 3. Top: "bulk" contribution to the XPS intensity (expression (8)) as a function of the sputtered thickness for several particle sizes. Bottom: "surface" contribution (expression (5)).

calculated by the following integral extended to all the particles that before the sputtering had their top face within the sample depth $a$.

$$I'_{bl} \alpha Dd^2 \int_0^a [1 - \exp((a - y - d)/\lambda_m)]dy \quad (6)$$

$$I'_{bl} \alpha Dd^2 [a + \lambda_m(\exp(-d/\lambda_m - \exp((a - d)/\lambda_m))]. \quad (7)$$

The total contribution of the bulk of catalyst can be calculated as the sum of expressions (7) and (3), the latter representing the particles which are still covered by the support:

$$I'_b \alpha Dd^2 [a + \lambda_m(\exp(-d/\lambda_m) - \exp((a - d)/\lambda_m) + \lambda_s(1 - \exp(-d/\lambda_m)]. \quad (8)$$

At any stage in the sputtering process for $a < d$ the sum of expressions (5) and (8) gives the total intensity of the photoelectron peak. However, if a sample depth $a > d$ has been sputtered, expression (8) gives the steady-state intensity since, under such conditions, all the particles initially at the surface have been removed and expression (5) vanishes.

Figure 3 shows a separate representation of expressions (8) and (5) in function of the sputtered thickness $a$ for several sizes of the particles of the dispersed phase.

Meanwhile, the representation in Fig. 4 of the sum of expressions (5) and (8), would correspond to the experimental sputtering profiles of the catalyst samples. For these representations the parameters $A$ and $D$ in (5) and (8) have been calculated according to expressions (A3) and (A9), the values corresponding to a $Ni/SiO_2$ catalyst with a metal load of 4% and a silica support of $S_{bet} = 200\ m^2g^{-1}$ taken for the different variables in these expressions.

Several questions from these two latter figures deserve a comment. First, the discontinuity appearing in the profiles at $a = d$, corresponding to the point where the particles at the surface have been completely removed, can be taken as a measure of the size of particles in a particular catalyst. Sec-

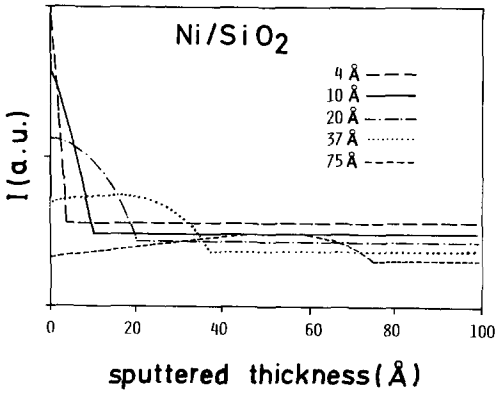


FIG. 4. Normalized depth profiles as a function of the sputtered thickness calculated for several sizes of the particles of the dispersed phase for a $Ni/SiO_2$ catalyst.

ond, the contribution of the particles in the bulk increases to reach its maximum for the steady state, just at $a = d$. This reflects the fact that particles originally embedded in the support (bulk particles) are progressively exposed by the ion etching and contribute without attenuation to the intensity of the peak. A third point to be stressed in these representations is that, for a given loading of the dispersed phase, the intensity in the steady state decreases when the particle size increases. This provides a test to assess relative particle sizes in a set of catalysts. This test can be used in addition to the traditional method of comparing the XPS intensities of the dispersed phase (*18–20*). In addition, the trend of the steady-state intensities can also be used to differentiate between an increase in particle size or formation of a solid solution (see below), two situations that lead to a decrease in the initial intensity of the photoelectron peaks and that are common for supported oxides. These considerations stand for the case of no preferential sputtering between the dispersed phase and the support. If preferential sputtering exists the profiles would change, so that their "breakpoint" would be shifted to longer sputter times and the steady-state intensity would be higher when the material of the support is preferentially sputtered (the opposite behavior should be expected when the dispersed phase is preferentially sputtered).

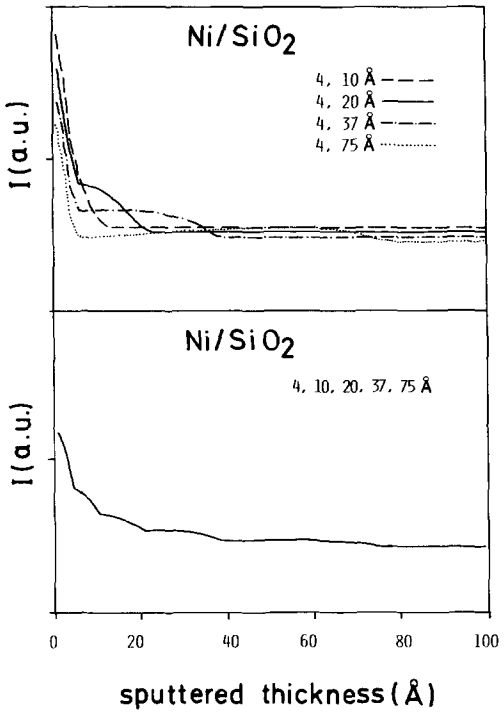


FIG. 5. Top: Normalized depth profiles calculated for a $Ni/SiO_2$ catalyst with different bimodal distributions of particles in the dispersed phase. Bottom: Normalized depth profile for a $Ni/SiO_2$ catalyst with five different sizes of particles in the dispersed phase.

*Model Calculations for Idealized Catalyst Structures*

(*a*) *Effect of the active phase distribution.* Starting from expressions (5) and (8) it is possible to simulate sputtering profiles of real catalysts by summation of different equations of this type, where the values of $d$ in each case correspond to those of the actual distribution of particle sizes in the catalyst.

A first situation corresponds to a catalyst with a narrow gaussian distribution of particle sizes around the value $d = a$. For such a case depth profiles similar to those in Fig. 4 are obtained where the sharp discontinuity appearing at $a = d$ is smeared out. Another example corresponds to the presence of a bimodal distribution of particles sizes, a situation which is sometimes difficult to ascertain by conventional methods, especially if the dispersed phase is not a metal and most of the available techniques for particle size determination cannot be used. However, the simulated profiles in Fig. 5, obtained for the same hypothetical $Ni/SiO_2$ catalysts, reveal that in certain cases bimodal distributions can be distinguished by this technique and that the size of the two types of particles can be assessed from the two points at which discontinuities appear in the depth profiles.

A simulation of a more complex particle size distribution is also shown in Fig. 5 for a catalyst with an equal number of particles of five different sizes between a $D_{min} = 4$ Å

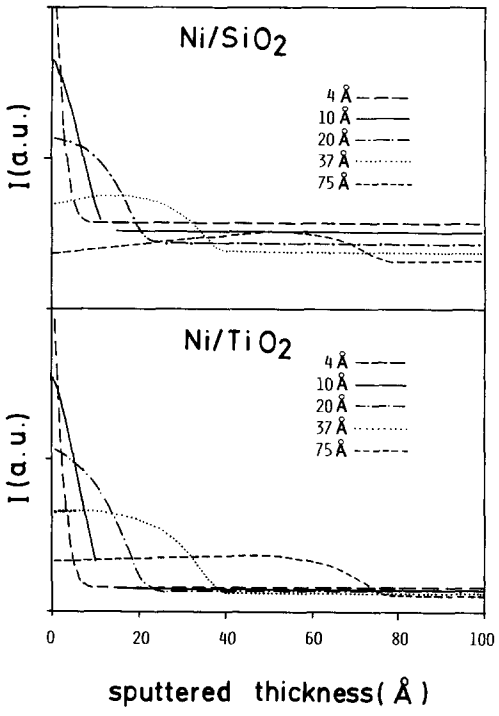


FIG. 6. Normalized depth profiles calculated for $Ni/SiO_2$ and $Ni/TiO_2$ catalysts with the same sizes for the particles in the dispersed phase.

and $D_{max}$ = 75 Å. The calculated profile corresponds to the superposition of five curves presenting five discontinuity points, one for each particle size. For real catalysts with more complex particle size distributions these discontinuities would be smeared out, leading to a monotonic decay of the XPS intensity for increasing sputtering times. In this case, the slope of the profile will give a rough idea of the type of particle size distribution, smaller slopes being expected for catalysts with bigger particle sizes. In the case of catalysts with a broad Gaussian distribution of particle sizes the sputtering profile will be the result of the superposition of the curves for each particle size weighted by its partition fraction. The slope of such profiles should give an idea of the medium particle size existing in the sample.

(*b*) *The role of the support.* Up to now we have paid attention to the active phase, although it could also be interesting to test whether the type of support has any influence on the shape of the sputtering profiles. According to expressions (A3) and (A9) for the parameters $A$ and $D$ included in expression (8), it could be expected that two catalysts where the supports have different $S_{bet}$ and $\rho$ values will present different depth profiles even if the active phase presents similar characteristics (chemical nature, dispersion degree, etc). This can be seen in Fig. 6 where the calculated depth profiles for a second $Ni/TiO_2$ catalyst (metal loading 4% and $S_{bet}$ = 50 $m^2g^{-1}$) are compared with those of the $Ni/SiO_2$ catalyst already presented in Fig. 4 (metal loading 4% and $S_{bet}$ = 200 $m^2g^{-1}$). This comparison shows that while the relative decrease in intensity upon sputtering is more important for the catalyst with smaller surface area, the differences in the steady-state intensity depend to a greater extent on the particle size for the catalyst with higher surface area.

Another situation which can be assumed, in particular with supported oxide catalysts, is that a portion of the active phase forms a solid solution within the support (note that a catalyst where the carrier has a large microporosity can be taken as a solid solution if the dispersed phase is homogeneously dis-

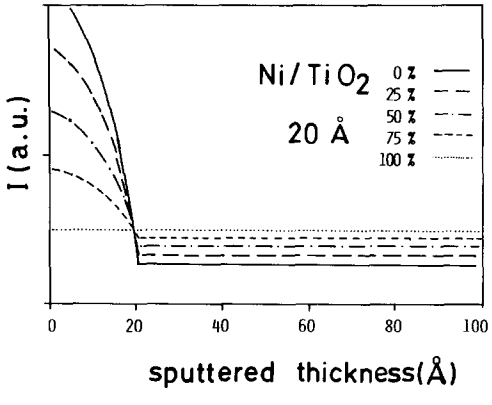


FIG. 7. Normalized depth profiles calculated for a $Ni/TiO_2$ catalyst with degrees of formation of a solid solution between 0 and 100%.

tributed through the micropores). The sputtering profiles in Fig. 7 correspond to this example for a size of the particles of the dispersed phase of $d = 20$ Å. The curves in this figure are the result of the sum of two terms, one corresponding to the particles of the dispersed phase distributed on the surface of the support grains (Eq. (8)), and another, corresponding to isolated atoms forming the solid solution. It is interesting that the steady-state intensity in Fig. 7 increases with the degree of solid solution, which is the opposite behavior to that found for increasing particle sizes (Fig. 4) (particles with small size would also lead to a higher intensity in the steady state but, while in this case the profile would be characterized by an initial sharp decrease in intensity, that of a solid solution would be flat).

## EXAMPLE APPLICATIONS

In the previous sections we have presented a model to describe the sputtering behavior of practical supported catalysts. This model provides semiquantitative information on different parameters of the dispersed phase, such as average particle size and formation of a solid solution. In this section we aim to validate the model with a series of examples which illustrate the possible applications of this technique for the characterization of catalysts.

### *Experimental*

We have studied a series of well-characterized catalysts which have been submitted sequentially to $Ar^+$ sputtering and XPS analysis.

The $Rh/TiO_2$ samples (2.5% by weight of rhodium) were prepared by wetness impregnation of $TiO_2$ (Degussa P-25, $50 \pm 1$ $m^2g^{-1}$) with a $RhCl_3$ solution. The dried precursor, in the following $RhCl_3/TiO_2$ sample, was reduced at 773 K in flowing hydrogen and then stored in air until its use. Further details on the preparation procedure and characterization of this sample (hereafter called $Rh/TiO_2$) have been given elsewhere (*21*).

The $Pt–Pd/TiO_2$ samples were prepared by photochemical deposition of platinum and palladium on $TiO_2$ Degussa P-25. A suspension of $TiO_2$ (500 mg) in a solution of hexachloroplatinic acid and palladium chloride was dearated under vacuum and irradiated under stirring for ca 24 h. Two different samples were prepared by this procedure, one containing 1.5% Pt and 1.85% Pd ($Pt–Pd/TiO_2$ sample) and another containing 1% Pd and 1% Pt ($Pt–Pd/TiO_2$-A sample). The different metallic loadings were obtained by changing the amount of the platinum and paladium salts in the solution. This leads to changes in the pH value of the medium which, in turn, controls the distribution of the two metallic phases in the $TiO_2$ support (*22*).

The $Pt/TiO_2$ samples (5% of metal by weight) were prepared by wetness impregnation of the same Degussa P-25 support with chloroplatinic acid. Once dried in flowing air at 383 K, the precursor was reduced at 773 K for 1 h, either in a dry hydrogen flow (sample $Pt/TiO_2$) or in a hydrogen flow with water vapor ($P = 0.036$ Torr) (sample $Pt/TiO_2–H_2O$). A careful study of the SMSI state in these two samples has been reported previously (*23*).

The $Ni/SiO_2$ samples have been prepared by wetness impregnation of $SiO_2$ (Aerosil 200 from Degussa) with a $Ni(HCOO)_2$ solution (I samples), and by homogeneous precipitation with urea from a $Ni(NO_3)_2$ solution (H samples). The impregnated precursors, with ca 4% nickel by weight, were dried and calcined with flowing $O_2$ at 673 K for 4 h and then reduced in flowing $H_2$ at 773 K for 1 h. The adopted labeling of these samples has been $NiO/SiO_2$-I(H), for the oxidized precursors and $Ni/SiO_2$-I(H) for the reduced catalysts.

The experimental depth profiles have been obtained on a Leybold–Heraeus XPS spectrometer working with a constant pass energy at 50 eV. Except for the spectra of the Ni-containing samples, recorded with the Al$K\alpha$ radiation, the Mg$K\alpha$ source was used in all the cases. The spectra were stored in a H–P 1000 E computer where data

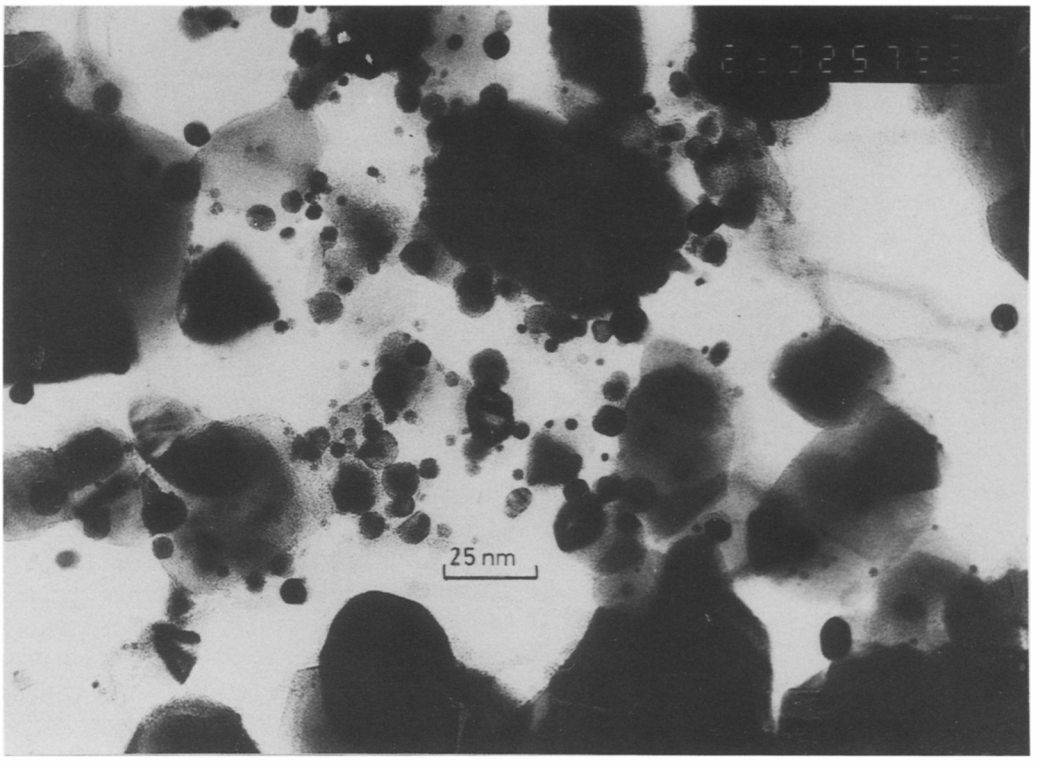


FIG. 8. TEM micrograph of the $Rh/TiO_2$ sample.

analysis was also carried out. This consists of background substraction and area calculation. The intensity of peaks of the dispersed phase is always referred to by the intensity of one peak of the support (Si(2*p*) and Ti(2*p*) in the studied samples), so that different samples can be compared. For convenience, in the depth profiles which are discussed together, these XPS intensities have been normalized to the maximum intensity of the profiles taken as 100, although the absolute value corresponding to the maximum of the scale is given in the caption of each figure. The maximum error estimated for all the measurements corresponds to 5% of the normalized scale.

Thermal treatments in the pretreatment chamber of the spectrometer were carried out by resistively heating a Mo holder on which pressed pellets of samples were placed.

Ion sputtering in this pretreatment chamber was carried out by means of a Peening ionization source supplied with Argon and working at 3.5 keV of accelerating voltage. Under these conditions calibration with a $Ta_2O_5$ standard (*24*) gave a sputtering rate of ca 12 Å $min^{-1}$.

TEM examination of samples was done with a JEOL 100C microscope, where STEM–EDX analysis was carried out with a STEM field emission gun (VGHB 501) equipped with a silicon–lithium diode detector (Link) and a multichannel analyzer (Tracor 500).

### *$Rh/TiO_2$: Formation of Metal Particles from a Precursor Salt*

The TEM micrograph of the $Rh/TiO_2$ sample in Fig. 8 shows the existence of Rh particles with sizes ranging between 20 and 100 Å, while the histogram of particles sizes

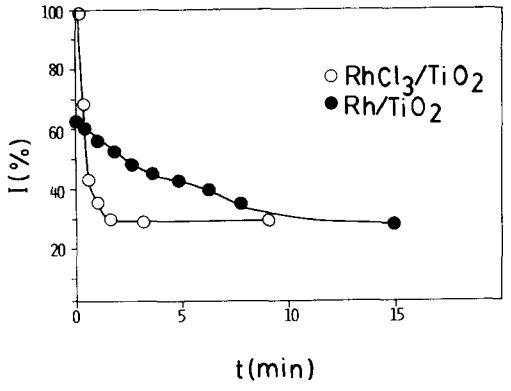


FIG. 9. Normalized depth profiles of the $Rh/TiO_2$ sample and its corresponding $RhCl_3/TiO_2$ precursor. The maximum at the scale (i.e., 100%) corresponds to $I_{Rh}/I_{Ti} = 13.1 \times 10^{-2}$ for the $RhCl_3/TiO_2$ sample).

reveals a maximum number of particles at ca 50 Å.

The sputtering profiles of sample $Rh/TiO_2$ and of its precursor, sample $RhCl_3/TiO_2$, are presented in Fig. 9. According to the model predictions, the sharply decaying profile of the precursor confirms that the rhodium ions must be highly dispersed on the surface of the support, being readily removed by sputtering for a few seconds. On the contrary, the less stepped profile of the $Rh/TiO_2$ catalyst is consistent with the presence of bigger particles formed by aggregation of the atoms of Rh during the reduction process. Moreover, according to our model, the steady state reached after sputtering for 5–8 min indicates the existence of rhodium particles with a size equivalent to the thickness of sample sputtered during this time. Taking into account the sputtering rate of our ion gun, a sample thickness of 60–90 Å has been removed during this time, a value that is in concordance with the maximum size of particles present in this sample (i.e., 100 Å). Also interesting is that the profile is more stepped during the first minutes of the etching process, a fact that points to the existence of small particles (i.e., smaller than 30–40 Å) whose removal is occurring during this initial period. This stresses the interest of the sputtering technique for systems with a heterogeneous distribution of the metallic phase.

*$Ni/SiO_2$: The Effect of Particle Size*

The $H_2$ chemisorption and XRD line broadening measurements of the $Ni/SiO_2$ catalysts gave an average particle size of ca. 30 and 300 Å, respectively, for the H and I samples (*17*). In agreement with these values, the different shape of the sputtering profiles in Fig. 10 indicate that quite different particle size distributions exist. Thus, for sample $Ni/SiO_2$-H the profile is characterized by a steady decay in intensity to reach a constant value for $t > 4$ min which, according to our model, suggests the existence of a broad distribution of small particles with $d < 50$ Å. On the contrary, sample $Ni/SiO_2$-I presents an initially increasing and then flat profile that could be associated with the big particles of Ni existing in this sample. However, it must be pointed out that an implicit assumption of the model is that the size of the particles of the dispersed phase is smaller than that of the particles of the support, a condition that is not held by this sample. In this regard, it is worth noting that the model predicts that the intensity in the steady state is smaller for samples with greater particle sizes, the opposite to that found when comparing the profiles of samples $Ni/SiO_2$-H and -I. Despite these facts, the profile obtained for sample $Ni/SiO_2$-I must be considered, on an empirical basis, as due to the big particles of nickel existing in this sample. Another interesting feature in Fig. 10 is the initial increase in intensity in the profiles of samples $Ni/SiO_2$-I, -H, and $NiO/SiO_2$-I, which is likely the result of some of the sputtering effects not considered in the model (i.e., preferential sputtering and roughening).

Figure 10 also shows that the sputtering profiles of the $NiO/SiO_2$-H precursor follows a trend parallel to that of its corresponding $Ni/SiO_2$-H sample. This indicates that the dispersion state of the active phase in this precursor is similar to that of the reduced samples. In addition, this trend

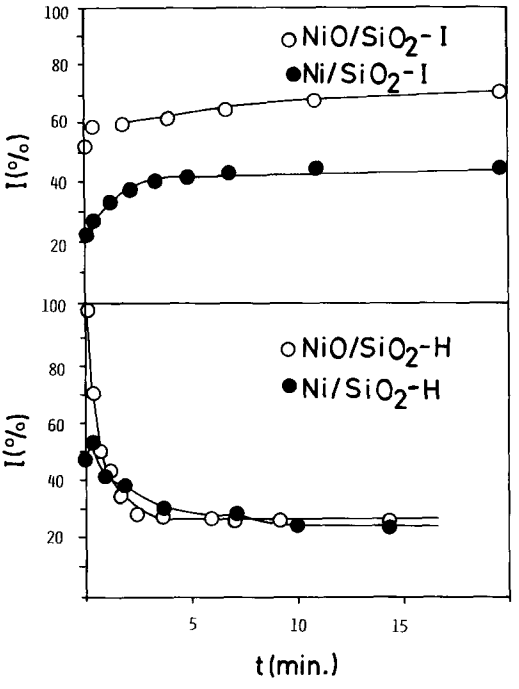


FIG. 10. Normalized depth profiles of the $Ni/SiO_2$ samples and their corresponding $NiO/SiO_2$ oxide precursors. The maximum at the scale (i.e., 100%) corresponds to $I_{Ni}/I_{Si} = 20.76 \times 10^{-1}$ for the $NiO/SiO_2$-H sample.

shows that the sputtering technique can be used to estimate the dispersion degrees for active phases in oxidized or other forms where conventional techniques for characterization of metallic catalysts cannot be utilized. In this figure it is also observed that the profile of sample $NiO/SiO_2$-I is parallel to that of sample $Ni/SiO_2$-I, although with a higher intensity in the steady state. This fact might also be associated with the problem mentioned above of the presence of too big particles of the dispersed phase. However, differences in the texture and/or the different distribution of the active phase (segregation) in both samples can also contribute to this behavior as we have recently shown with a series of $Rh/CeO_2$ catalysts (*25*).

### *Pt–Pd/TiO₂: The Formation of Bimetallic Particles*

Micrographs of the two Pt–Pd bimetallic catalysts are presented in Fig. 11. For the Pt–Pd/$TiO_2$ sample the TEM/STEM analysis shows the formation of big particles of Pt at the grain edges in the form of particle aggregates and sponges, as well as small separate particles of Pd with sizes ranging between 20 and 50 Å. On the contrary, for the Pt–Pd/$TiO_2$-A catalyst, formation of two types of bimetallic particles, of 8–10 Å and ca. 30 Å in size, the latter much less abundant, is revealed by TEM–STEM. The depth profiles in Fig. 12, for example Pt–Pd/$TiO_2$, show that the XPS intensity of these two elements decreases differently with the sputtering time. However, parallel profiles for Pt and Pd are obtained, for example Pt–Pd/$TiO_2$-A, where bimetallic particles have been detected by TEM–STEM (however, it must be noted that a similar behavior would have been observed for separate Pd and Pt particles of the same size).

On the other hand, the shapes of the two profiles support the general conclusions of our model, the higher intensity at the steady state for Pt and Pd in the Pt–Pd/$TiO_2$-A catalyst being consistent with smaller particle sizes. In addition, for both samples, the initial sharp decay of the intensity is consistent with the presence of very small particles of Pt and Pd on the surface of the support, besides the particles observed by TEM of sizes ranging between 10 and 50 Å.

### *Pt/TiO₂: The Burial of the Metal Particles by the Support*

A full study of Pt/$TiO_2$ and Pt/$TiO_2$–$H_2O$ samples in relation to the strong metal support interaction (SMSI) effect has been reported previously (*23*). In that work, the characterization by $H_2$ chemisorption and XRD of the metal dispersion state of Pt shows that while particles of less than 20 Å exist in sample Pt/$TiO_2$, bigger particles of ca. 70 Å are formed in Pt/$TiO_2$–$H_2O$ where the $H_2$ adsorption is practically suppressed because of the SMSI state. The depth profile in Fig. 13 of sample Pt/$TiO_2$, characterized by a stepped decay in the XPS intensity after sputtering for a few seconds, is consistent with the existence of small platinum particles at the surface of the support, whose

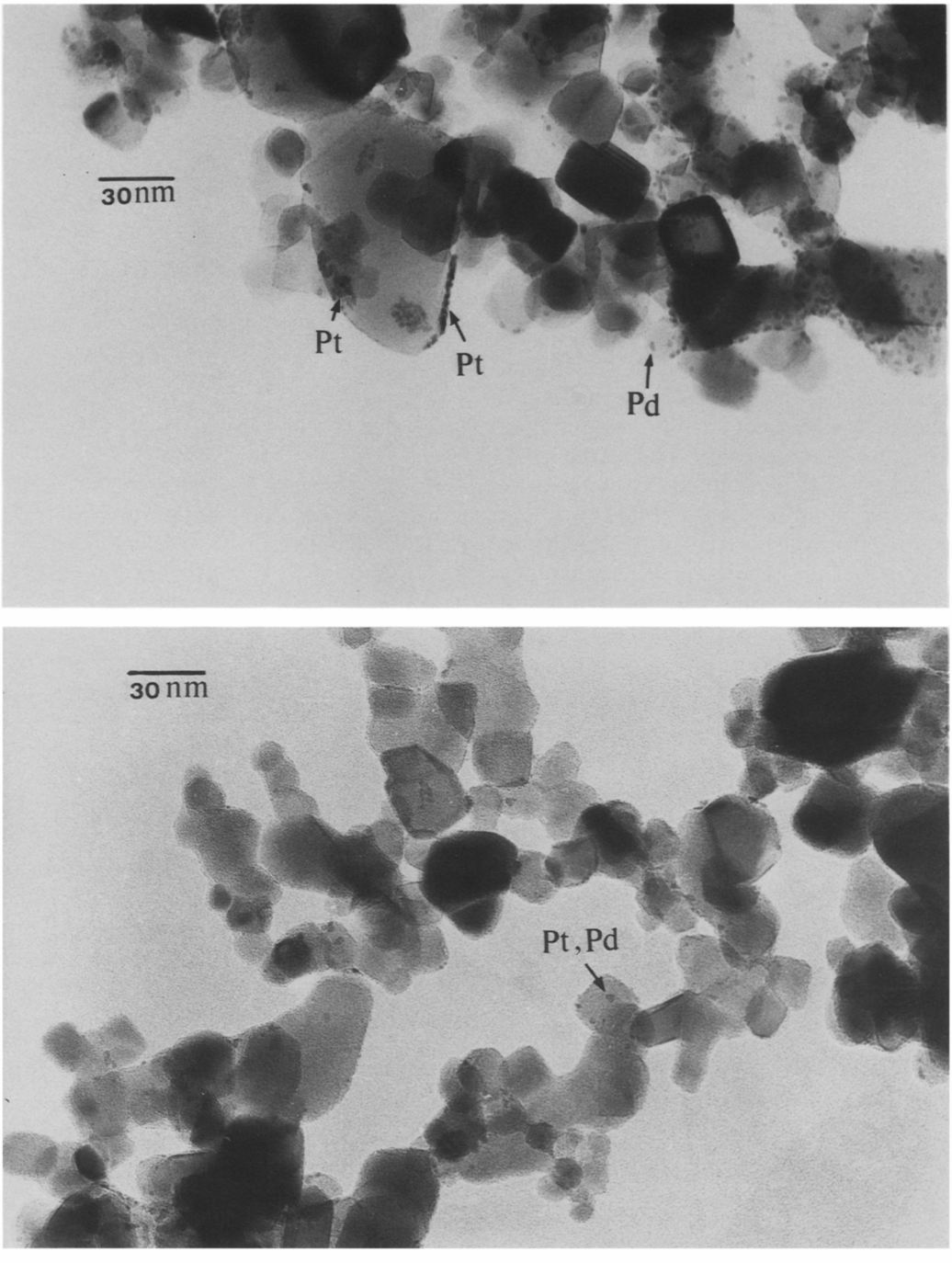


FIG. 11. Top: TEM micrograph of the Pt–Pd/$TiO_2$ catalyst; Pt or Pd particles are indicated by arrows. Bottom: TEM micrograph of the Pt–Pd/$TiO_2$-A catalyst; the bimetallic particles existing in this catalyst are indicated by arrows.

removal is readily attained by $Ar^+$ etching. However, the depth profile of sample Pt/$TiO_2$–$H_2O$ does not adjust exactly to that expected for catalysts with metal particles of ca. 70 Å. According to our model, depth profiles of a sample with particles of that size should be characterized by an initial and steady slow increase and a sharp decrease in intensity after etching a sample thickness similar to the metal particle size (i.e., 70 Å). This is not found for the profile of sample Pt/$TiO_2$–$H_2O$, which only shows a steady increase in intensity to reach a constant value after 3–4 min (i.e., corresponding to a sample thickness of 35–50 Å according to the sputtering rate of the $Ta_2O_5$ standard). However, this shape could be the result of the convolution of such a profile with that resulting from the burial of the platinum particles in the bulk of the support, so that they would be exposed only after the removal of a thickness of support of approximately 35 Å. This full encapsulation of the Pt particles was proposed in our previous work (*23*) based on the fact that in the unetched Pt/$TiO_2$–$H_2O$ sample the Pt was not oxidized by exposure to $O_2$ at 673 K, whereas in the etched sample oxidation of Platinum occured already at 473 K. To explain this result we assumed that during the activation of the precursor in wet $H_2$ two effects took place for Pt/$TiO_2$–$H_2O$ (*26*), the first is that water induces the agglomeration of the metal atoms during reduction. The second is the mobilization of the support enhanced by the simultaneous presence of water and $H_2$, to fully cover the metal particles. An enhancement of the mobilization of supported oxides by the presence of water has been reported by Knözinger and co-workers (*27*) for $MoO_3$ and $V_2O_5$ under oxidizing conditions. However, the effect reported here and in our previous work (*23*) refers to a similar mobilization effect but under a reducing atmosphere. Although this effect must be explored in more detail, it is likely that hydroxylation of the $TiO_2$ by the water could contribute to the spillover of hydrogen to the support where, as we have shown previously (*28*), it forms $TiO_x$-H like species which present a specific effect on the enhancement of the ionic mobility of the lattice components.

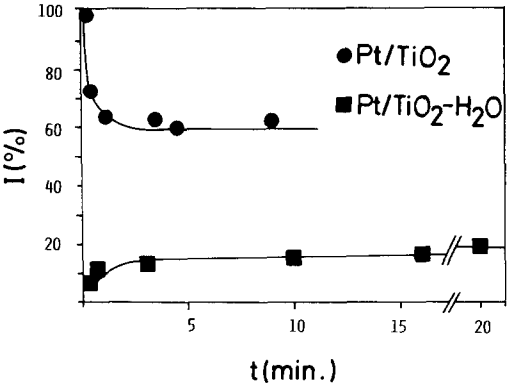


FIG. 13. Depth profiles of $Pt/TiO_2$ and Pt/$TiO_2$–$H_2O$ samples. The maximum at the scale (i.e., 100%) corresponds to $I_{Pt}/I_{Ti} = 12.3 \times 10^{-2}$ for the $Pt/TiO_2$ sample.

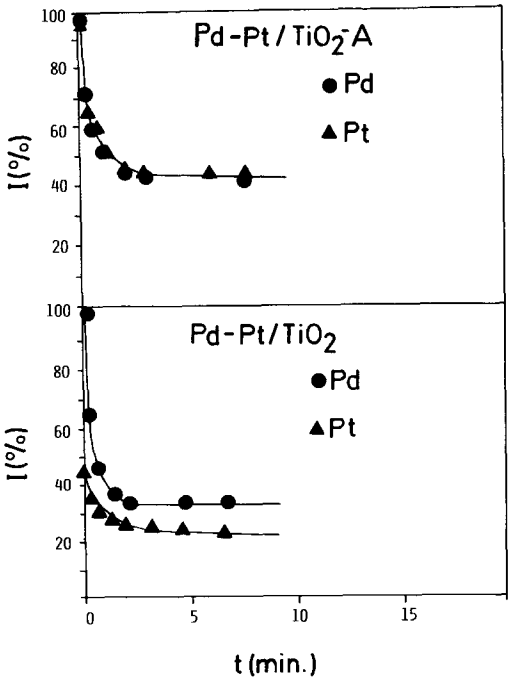


FIG. 12. Normalized depth profiles of Pt–Pd/$TiO_2$ and Pt–Pd/$TiO_2$-A samples. The maxima at the scales (i.e., 100%) correspond to $I_{Pd}/I_{TI} = 8.4 \times 10^{-2}$ for Pt–Pd/$TiO_2$ and $I_{Pt(Pd)}/I_{Ti} = 3.1 \times 10^{-2}$ for Pt–Pd/$TiO_2$-A.

## CONCLUSIONS

In this paper a model is elaborated to describe the effect of ion sputtering on polycrystalline materials composed of two phases, a carrier and a dispersed phase, the latter generally in the form of small supported particles on its surface. The implications of this model in catalyst characterization are highlighted by some examples showing the possibilities of the method. From the different experimental results it is clear that the method can be very fruitful for the study of either precursor samples, where most of the available techniques for metallic catalyst characterization cannot be applied, or catalyst with the dispersed phase in metallic state. Upon calibration of the sputtering rate of the experimental apparatus, semiquantitative information on particle size (dispersion state of the active phase), heterogeneity of the active phase, or the existence of total or partial solid solution may be deduced by this method. For bimetallic catalysts the possible formation of mono- or bimetallic particles can also be distinguished, provided that in the first case the particles of the two metals present different particle sizes.

## APPENDIX: NUMBER OF PARTICLES OF THE DISPERSED PHASE AT THE "SURFACE" AND IN THE "BULK" OF THE IDEALIZED CATALYST STRUCTURE

To estimate the concentration of particles of the dispersed phase exposed on the surface of the catalyst and that, therefore, are directly seen by the EEA, the closed packet arrangement of spheres in Fig. A1 can be taken as an approximate description of the agglomerates of (generally non-uniform) particles of the support in a catalyst sample. Assuming no microporosity, the radius of these spheres is given by

$$r = 3/S_{\text{bet}}\,\rho. \qquad \text{(A1)}$$

In this arrangement, those particles of the dispersed phase located in the zone A can be considered as being the particles exposed on the surface in Fig. 1, while those located

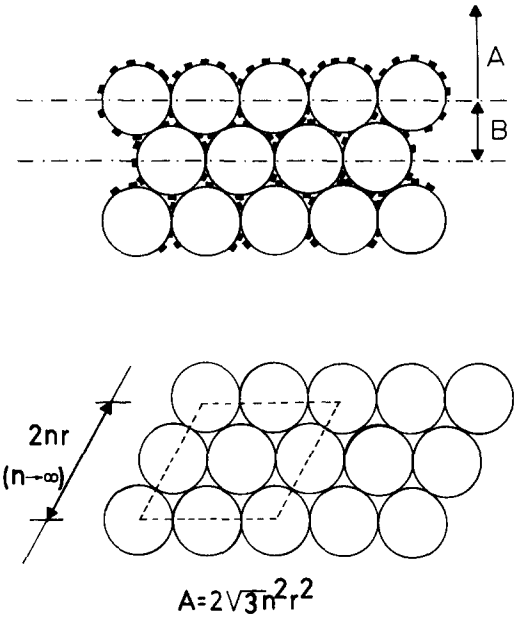


FIG. A1. Idealized closed-packed arrangement of particles for a supported catalyst. (a) Side view. (b) Top view.

in zone B and beneath belong to the bulk of the idealized catalyst structure in that figure. For a unit area of this arrangement, and considering that the radius of the spheres is very small compared with the geometrical dimensions of the region seen by the EEA, the calculated number of spheres per unit area is $(2\sqrt{3}\,r^2)^{-1}$.

From Fig. A1 it is also possible to calculate the number of atoms of the active phase in zone A per unit area of catalyst sample seen by the EEA. This number is given by

$$n' = (2r^2\pi\,\rho_s n^2)/(2\sqrt{3}n^2r^2) = (1/\sqrt{3})\pi\,\rho_s, \qquad \text{(A2)}$$

where the number of atoms is calculated for $n^2$ hemispheres of zone A and referred to the macroscopic area of the sample containing these spheres ($2\sqrt{3}\,n^2\,r^2$; see Fig. A1).

From expression (A2) the number of particles of the dispersed phase is then

$$A = n'/d^3\,D_m = \pi\rho_s/(\sqrt{3}\,d^3D_m). \qquad \text{(A3)}$$

In the same way the number of atoms of the dispersed phase existing in zone B is

$$n'' = 2n' = (2/\sqrt{3})\pi\rho_s \quad \text{(A4)}$$

and the number of particles of the dispersed phase

$$N = n''/d^3D_m = 2\pi\rho_s/(\sqrt{3}d^3D_m). \quad \text{(A5)}$$

These atoms will be embedded in an effective volume of the support which can be taken as equivalent to the volume of hemispheres in zone B. The volume of these hemispheres per unit area of sample surface seen by the EEA is

$$Ve = 2n^2\ V \text{ hemispheres} = (4/3)\ n^2\pi r^3. \quad \text{(A6)}$$

Whence the effective thickness of zone B can be defined as

$$Te = \text{Ve/Area} = (4/3)(n^2\pi r^3)/(2\sqrt{3}n^2r^2) = 2\pi r/(3\sqrt{3}). \quad \text{(A7)}$$

Assuming, as in Fig. 1b, a homogeneous distribution of particles within the bulk of the idealized catalyst structure, it is possible to write the following expression for the number of particles in zone B, including the number of particles of the dispersed phase with their top surface in $dy$ at a distance $y$ from the surface ($D$).

$$N = 2\pi\rho_s/(\sqrt{3}d^3D_m) = \int_0^{Te} D\,dy \quad \text{(A8)}$$

and

$$D = 3\rho_s/(d^3D_m r) = S_{bet}\rho\rho_s/(d^3D_m). \quad \text{(A9)}$$

The values of $A$ and $D$ thus calculated refer to the surface and bulk contribution to the profiles under the assumption of a homogeneous distribution of the active phase particles on the surface of the support particles. Other situations where there is enrichment in the pores or in the external surface of the sample (e.g., in the case of extrudates) would lead to relatively higher values of, respectively, $D$ and $A$. In these cases a theoretical simulation of the experimental profiles by changing the values of $D$ and $A$ could give some information on the possible inhomogeneities in the studied samples. This question has been addressed by us in a recent work on $Rh/CeO_2$ catalysts (*25*).

ACKNOWLEDGMENTS

Financial support from the CICYT (project n.Mat88-0223) is acknowledged. One of us (A.R.G.E.) thanks the Alexander von Humboldt foundation and the Max Planck Gesellschaf for grants which enabled the realization of part of this work. Helpful discussions with Prof. S. Hoffman from the IMF (Stuttgart) are also acknowledged. We also thank C. Leclerq from the "Institut de Recherches sur la Catalyse" for the TEM micrographs and Dr. J.-M. Herrmann for the Pt–Pd samples.

REFERENCES

1. Hofmann, S., Surf. *Interface Anal.* **2,** 148 (1980).
2. Benninghoven, A., *Z. Phys.* **230,** 403 (1970).
3. Carter, G., Navinsek, and B., Whiton, J. L., *in* "Sputtering by particle Bombardment" (R. Behrisch, Ed.), p. 231. Springer-Verlag, Heidelberg, 1983.
4. Ho, P. S., Lewis, J. E., Wildman, H. S., and Howard, J. K., *Surf. Sci.* **57,** 383 (1976).
5. Scherzer, B. M. U., *in* "Sputtering by Particle Bombardment" (R. Berisch, Ed.), p. 271. Springer-Verlag, Heidelberg, 1983.
6. Sanz, J. M., and Hofmann, S., *Surf. Interface Anal.* **8,** 147 (1986).
7. Hofmann, S., and Sanz, J. M., *Surf. Interface Anal.* **6,** 78 (1984).
8. Seah, M. P., Sanz, J. M., and Hofmann, S., *Thin Solid* Films **81,** 239 (1989).
9. Margraf, R., Knözinger, H., and Taglauer, E., *Surf. Sci.* **211/212,** 1083 (1989).
10. Maezawa, A., Okamoto, Y., and Imanaka, T., *J. Chem. Soc. Faraday Trans.* **83,** 665 (1987).
11. Munuera, G., González-Elipe, A. R., Espinós, J. P., Muñoz, A., Conesa, J. C., Soria, J., and Sanz, J., *Catal. Today* **2,** 663 (1988).
12. Hochella, M. F., Lindsay, G. R., Mossotti, V. G., and Eggleston, C. M., *Am. Miner.* **73,** 1449 (1988).
13. González-Elipe, A. R., Martínez-Alonso, A., and Tascón, G. M. D., *Surf. Interface Anal.* **12,** 565 (1988).
14. Henrich, V. E., and Fan, J. C. C., *Surf. Sci.* **42,** 139 (1974).
15. Cross, Y. M., and Dewing, G., *Surf. Interface Anal.* **1,** 27 (1979).
16. Nyborg, L., Nylund, A., and Olefkord, I., *Surf. Interface Anal.* **12,** 110 (1988).
17. González-Elipe, A. R., Munuera, G., and Espinós, J. P., *Surf. Interface Anal.* **16,** 375 (1990).
18. Kerkhof, F. P. J. M., and Moulijn, G. A., *J. Phys. Chem.* **83,** 1613 (1979).
19. Kuipers, H. P. C. E., van Leuven, H. C. E., and Visser, W. M., *Surf. Interface Anal.* **8,** 235 (1986).

20. Mark Davis, S., *J. Catal.* **117,** 432 (1989).

21. (a) Conesa, J. C., Malet, P., Munuera, G., Sainz, M. T., Sanz, J., and Soria, J., *in* "Proceedings, 8th International Congress on Catalysis, Berlin, 1984," Vol. 5, p. 217. Dechema, Frankfurt-am-Main, 1984; (b) Gonzalez-Elipe, A. R., Munuera, G., Espinos, J. P., Muñoz, A., and Fernandez, A., *in* "E-MRS Meeting," Vol. XV, p. 587, 1988.

22. Fernandez, A., Munuera, G., Gonzalez-Elipe, A. R., Espinos, J. P., Herrmann, J. M., Pichat, P., and Leclerq, C., *Appl. Catal.* **57,** 191 (1990).

23. Gonzalez-Elipe, A. R., Malet, P., Espinos, J. P., Caballero, A., and Munuera, G., *Stud. Surf. Sci. Catal.* **48,** 427 (1989).

24. Sanz, J. M., and Hofmann, S., *Surf. Interface Anal.* **5,** 210 (1983).

25. González-Elipe, A. R., Alvarez, A., Holgado, J. P., Fernández, A., Espinós, J. P., and Munuera, G., *in* "Fundamental Aspects of Heterogeneous Catalysts by Particle Beams" (H. H. Brongersma and R. A. Van Santen, Eds.), Plenum, New York, in press.

26. Raupp, G. B., and Delgass, W. N., *J. Catal.* **58,** 337 (1979).

27. Leyrer, J., Margraf, R., Taglauer, E., and Knözinger, H., *Surf. Sci.* **201,** 603 (1988).

28. Munuera, G., González-Elipe, A. R., Espinós, J. P., Conesa, J. C., Soria, J., and Sanz, J., *J. Phys. Chem.* **91,** 6625 (1987).